Journal of Magnetic Resonance 255 (2015) 122–131

Contents lists available at ScienceDirect

Journal of Magnetic Resonance

journal homepage: www.elsevier.com/locate/jmr

Characterising the rheology of non-Newtonian fluids using PFG-NMR and cumulant analysis

T.W. Blythe [a], A.J. Sederman [a,*], J. Mitchell [a,1], E.H. Stitt [b], A.P.E. York [c], L.F. Gladden [a]

[a] Magnetic Resonance Research Centre, Department of Chemical Engineering and Biotechnology, University of Cambridge, Pembroke Street, Cambridge CB2 3RA, UK
[b] Johnson Matthey Technology Centre, Billingham TS23 1LB, UK
[c] Johnson Matthey Technology Centre, Blounts Court, Sonning Common, Reading RG4 9NH, UK

ARTICLE INFO

Article history:
Received 13 January 2015
Revised 16 March 2015
Available online 11 April 2015

Keywords:
PFG
Rheology
Cumulant analysis
Complex fluid
Propagator

ABSTRACT

Conventional rheological characterisation using nuclear magnetic resonance (NMR) typically utilises spatially-resolved measurements of velocity. We propose a new approach to rheometry using pulsed field gradient (PFG) NMR which readily extends the application of MR rheometry to single-axis gradient hardware. The quantitative use of flow propagators in this application is challenging because of the introduction of artefacts during Fourier transform, which arise when realistic sampling strategies are limited by experimental and hardware constraints and when particular spatial and temporal resolution are required. The method outlined in this paper involves the cumulant analysis of the acquisition data directly, thereby preventing the introduction of artefacts and reducing data acquisition times. A model-dependent approach is developed to enable the pipe-flow characterisation of fluids demonstrating non-Newtonian power-law rheology, involving the use of an analytical expression describing the flow propagator in terms of the flow behaviour index. The sensitivity of this approach was investigated and found to be robust to the signal-to-noise ratio (SNR) and number of acquired data points, enabling an increase in temporal resolution defined by the SNR. Validation of the simulated results was provided by an experimental case study on shear-thinning aqueous xanthan gum solutions, whose rheology could be accurately characterised using a power-law model across the experimental shear rate range of 1–100 s^{-1}. The flow behaviour indices calculated using this approach were observed to be within 8% of those obtained using spatially-resolved velocity imaging and within 5% of conventional rheometry. Furthermore, it was shown that the number of points sampled could be reduced by a factor of 32, when compared to the acquisition of a volume-averaged flow propagator with 128 gradient increments, without negatively influencing the accuracy of the characterisation, reducing the acquisition time to only 3% of its original value.

1. Introduction

Rheological characterisation using nuclear magnetic resonance (NMR) typically utilises spatially-resolved measurements of velocity to characterise local shear rates [1]. However, accurate rheological characterisation requires the accurate measurement of velocity and the corresponding pressure drop, with the range of shear rates that the data is accurate over sensitive to a combination of the velocity resolution, number of spatially-resolved data points, and flow properties [2]. The accuracy of the measured velocity data is sensitive to a combination of the signal-to-noise ratio (SNR) and the number of spatially-resolved data points. Depending on the system under study, over 100 spatially-resolved velocity data points might be required [3]. Conventional imaging techniques limit the temporal resolution of this approach and although a number of fast imaging techniques exist [4–6], many of these are unable to provide the spatial resolution required. To this end, and with a transition to low field hardware in mind, recent research has focused on developing new acquisition and analysis strategies enabling flow [7] and rheological characterisation [8] in real-time. Many of these strategies are indirect measurements of flow, exploiting the sensitivity of spin–spin relaxation times to translational motion [9,10].

Phase encoding NMR techniques offer an alternative method of (direct) velocity characterisation and are perhaps the most robust and quantitative way of measuring flow [11]. Molecules

* Corresponding author.
E-mail address: ajs40@cam.ac.uk (A.J. Sederman).
[1] Current address: Schlumberger Gould Research, High Cross, Madingley Road, Cambridge CB3 0EL, UK.

http://dx.doi.org/10.1016/j.jmr.2015.03.015
1090-7807/© 2015 The Authors. Published by Elsevier Inc.

experiencing coherent motion, i.e. flow, will accrue a phase shift proportional to their displacement, ζ, during an observation time, Δ, with the residual phase shift (ϕ) equal to $\gamma g \delta \zeta$, where γ is the gyromagnetic ratio and δ and g the duration and magnitude of the flow-encoding gradient, respectively, applied along a single axis parallel to the direction of flow. Note that displacement and velocity, v, may be used interchangeably, where $\zeta = v\Delta$. The signal is sampled in q-space, defined as $q = (1/2\pi)\gamma g\delta$, with q-space traversed either by increasing the duration or the magnitude of the flow-encoding gradient [11].

Early work by Packer [12] theoretically investigated the effect of coherent motion on the NMR signal for a static flow-encoding gradient, i.e. with Δ equal to δ such that $\phi = \gamma v g \delta^2$. The effect was validated experimentally to characterise a single-velocity flow system. For multiple-velocity flow systems, the acquired signal in q-space is a superposition of signals from each isochromat of nuclear spins, each possessing a different phase shift. Fourier transformation of the signal in q-space yields a displacement, or velocity, probability distribution that completely characterises the flow under study [13]. This was utilised by Grover and Singer [14] to characterise the velocity probability distribution of flow through a human finger, and later by Garroway [15] for water flow through a cylindrical pipe. More recent technique developments in this area have also been made [16].

The use of volume-averaged displacement probability distributions for rheological characterisation was theoretically described by McCarthy et al. [17], and qualitative experimental agreement was later demonstrated for a range of Newtonian and non-Newtonian fluids [18]. Despite recent efforts [19], the quantitative use of displacement probability distributions remains challenging. We introduce a new approach utilising pulsed field gradient (PFG) NMR and cumulant analysis to enable the characterisation of power-law fluids, during flow, using only a single-axis gradient system. The removal of spatial encoding increases the SNR associated with the measurement.

PFG-NMR is a phase encoding technique involving the application of pulsed flow-encoding gradients with increasing (or decreasing) magnitude, in conjunction with spin echoes [20] or stimulated echoes [21], to traverse q-space. The signal acquired in q-space, $S(q)$, incorporates both coherent and incoherent motion, with the latter responsible for an attenuation of the signal due to a distribution of phase [20]:

$$S(q) \propto \int p(\zeta) e^{i2\pi q\zeta - 4\pi^2 D\left(\Delta - \frac{\delta}{3}\right)q^2} \mathrm{d}\zeta, \tag{1}$$

where $p(\zeta)$ represents the displacement probability distribution, or flow propagator [22], and D the molecular self-diffusivity. The signal in q-space and the displacement probability distribution are mutually conjugate Fourier pairs, and so Fourier transformation of $S(q)$ yields $p(\zeta)$. This approach is developed here to enable characterisation of the flow behaviour index, n, describing the non-linear contribution to the stress response of a non-Newtonian fluid subjected to deformational flow. For a power-law fluid:

$$\tau(\dot{\gamma}) = k\dot{\gamma}^n, \tag{2}$$

where τ and $\dot{\gamma}$ represent the shear stress and shear rate, respectively, and k is the consistency index. Perturbations in the flow behaviour index can be responsible for considerable changes in fluid behaviour and, therefore, the characterisation and monitoring of such behaviour is critical to many industrial flow processes, including spraying, mixing, and coating [23]. Using simple fluid mechanics it can be shown that, for flow through a cylindrical pipe, the displacement at radial position r is given by:

$$\zeta(r) = \langle\zeta\rangle\left(\frac{3n+1}{n+1}\right)\left(1 - \left(\frac{r}{R}\right)^{\frac{n+1}{n}}\right), \tag{3}$$

where $\langle\zeta\rangle$ is the mean fluid displacement and R is the radius of the pipe. Fig. 1 shows displacement profiles for three fluids, and demonstrates a reduction in the maximum displacement as the flow behaviour index is reduced. It follows that perturbations in the flow behaviour index will therefore be expected to induce changes in the flow propagator, and this is exploited in this work.

The q-space vector has dimensions of reciprocal length and so the increment in q defines the field-of-flow (FOF) and the range of q-space sampled defines the resolution of the flow propagator. To obtain the displacement probability distribution without the introduction of artefacts during Fourier transform, $S(q)$ is required to be sampled at adequate density, defined by the FOF, and over a sufficient range of q-space such that the signal approaches zero. Gradient strength limitations and spin relaxation times restrict the range of q-space accessible and so the introduction of truncation artefacts during Fourier transform may be experimentally unavoidable. Furthermore, the long acquisition times associated with such sampling requirements, typically of the order of tens of minutes, prevent the real-time characterisation of non-Newtonian fluids using magnetic resonance. In this paper, we develop a cumulant analysis approach eliminating these requirements, and thus removing the prohibitively long acquisition times.

Cumulant analysis has previously been used in the NMR community to analyse the flow of Newtonian and non-Newtonian fluids at low SNR [24,25]. Here we extend and apply these methodologies to characterise the flow behaviour index of power-law fluids. The signal in q-space may be approximated, over low-q, by the power series expansion of the cumulant-generating function:

$$\ln S(q) = \sum_{j=1}^{\infty} \frac{(iq)^j}{j!} X_j, \tag{4}$$

where X_j corresponds to the j^{th} cumulant. Upon expansion of Eq. (4), even powers of q give the log-magnitude of the signal, while odd powers of q give the phase of the signal. The signal in q-space is non-Gaussian and so cumulants above second order can be extracted. If cumulants are known for a suitable range of flow behaviour indices, with given experimental parameters, calculation of the flow behaviour index is possible through comparison of the experimental cumulants with those obtained numerically. Furthermore, the error associated with a cumulant may be determined by performing a non-linear regression across an increasing range of q-space, as outlined by Scheven et al. [25], with the standard deviation of the cumulants providing a measure of the error. The robustness of cumulant analysis to SNR is exploited in this work to determine the minimum data needed to characterise the flow behaviour index with reasonable accuracy, here defined as ±5%, this error being typical of conventional rheometry methods [26]. Several variables may contribute to the accuracy of the characterisation; namely SNR, number of sampled q-space data points, and n characterising the fluid under study. These variables are investigated systematically using simulated NMR data. The relative contributions of each variable to the accuracy of the characterisation are also considered. Validation of the simulations is provided through an experimental study of non-Newtonian shear-thinning ($n < 1$) xanthan gum solutions and (Newtonian) water using NMR. Further validation is provided using conventional rheometry methods.

The technique developed here is model-dependent, and so caution must be taken to ensure the fluid under study demonstrates power-law rheology across the shear rate range of the system. Any deviation from power-law rheology would result in an increase in the error associated with the characterisation. In contrast, conventional rheometry and MRI velocity profiles [3] provide model-independent data, with a fit to an empirical model

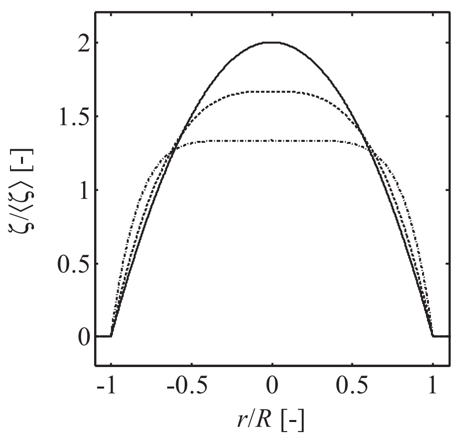

Fig. 1. Displacement (represented as a fraction of mean displacement) plotted as a function of radius (represented as a fraction of the pipe radius) for three examples of flow behaviour index; (—) $n = 1$, (- -) $n = 0.5$, and (-·-) $n = 0.2$. The displacement data were generated using Eq. (3).

performed at a later time (if required). Unlike MRI velocity profiles, however, the accuracy of the characterisation using PFG-NMR is independent of the shear rate range investigated, providing power-law rheology is maintained.

2. Model development

The analysis of acquisition data using cumulants first requires the simulation of $S(q)$ for a suitable range of n. Previous work by Kaiser et al. [27] generated $S(q)$ numerically using Eq. (1) for a finite spin ensemble of 10^4 spins. Here we use an analytical expression derived by McCarthy et al. [17] to describe $p(\zeta)$ as a function of the flow behaviour index, enabling the validation of numerical simulations. The details of the derivation are shown below.

The displacement, ζ, can be correlated to a range of radial distances, r, using:

$$r(\zeta) = R\left(1 - \frac{\zeta}{\zeta_{\max}(n)}\right)^{\frac{n}{n+1}}, \quad (5)$$

where $\zeta_{\max}(n)$, equal to $\zeta((2n+1)/(n+1))$, is the maximum fluid displacement. If we assume a homogeneous spin density, $p(\zeta)$ per unit length is proportional to the area of the flow field dA, with dA given by the differential of $A(\zeta)$, where $A(\zeta) = \pi r(\zeta)^2$, $p(\zeta)$ can be described as:

$$p(\zeta, n) \propto \frac{\mathrm{d}}{\mathrm{d}\zeta}\left(\pi R^2\left(1 - \frac{\zeta}{\zeta_{\max}(n)}\right)^{\frac{2n}{n+1}}\right). \quad (6)$$

We now drop the constant πR^2 for convenience and the evaluation of the differential in Eq. (6) yields an analytical expression describing the displacement probability distribution as a function of the flow behaviour index:

$$p(\zeta, n) = \begin{cases} \frac{1}{\zeta_{\max}(n)}\left(\frac{2n}{n+1}\right)\left(1 - \frac{\zeta}{\zeta_{\max}(n)}\right)^{\frac{n-1}{n+1}}, & 0 < \zeta < \zeta_{\max}, \\ 0, & \zeta_{\max} \leqslant \zeta. \end{cases} \quad (7)$$

Equations describing the displacement probability distribution for fluids demonstrating Newtonian, plug flow, and Bingham plastic behaviour may be found in the literature [17,18]. Fig. 2(a) shows the displacement probability distributions for the three examples of flow behaviour index considered in Fig. 1; it is seen that a reduction in n is responsible for a reduction in the maximum displacement and an increase in the maximum probability. These changes are due to a flattening of the flow profile with increasing n as shown in Fig. 1. When the constitutive equation describing the rheological behaviour of the fluid under study does not allow the analytical differentiation of Eq. (6), $p(\zeta, n)$ can be determined numerically.

Experimentally, the outflow of spins will lead to some loss of signal, with the amount lost related to the displacement, or velocity. To account for this, a correction is applied to the displacement probability distributions given by:

$$p'(\zeta, n) = (1 - \alpha)p(\zeta, n), \quad (8)$$

where $\alpha = \zeta/L$ and L is the length of the excitation region, and $p'(\zeta, n)$ represents the experimentally acquired displacement probability distribution. Eq. (8) must also be applied to the experimentally acquired flow propagators to recover $p(\zeta, n)$. The signal measured in q-space becomes:

$$\frac{S(q, n)}{S(0)} = \int p'(\zeta, n)e^{iq\zeta - 4\pi^2 D(\Delta - \frac{\delta}{3})q^2}\mathrm{d}\zeta. \quad (9)$$

As shown in Fig. 2(b), the changes in the displacement probability distributions observed in Fig. 2(a) cause a reduction in the frequency of the oscillation in q-space but an increase in the amplitude of the oscillation as n decreases. The existence of a relationship between the acquired signal and the flow behaviour index makes PFG-NMR an ideal tool for the characterisation of the flow behaviour index of fluids demonstrating power-law rheology; it is non-invasive and not limited by optical opacity, offering advantages over alternative imaging and sensor techniques. This is a model-dependent approach, and so holds true only for instances where the rheology of a fluid may be accurately described by the power-law empirical model across the range of shear rates investigated.

The log-magnitude and phase of the q-space signal, shown in Fig. 3 for the three examples of flow behaviour index, can be accurately approximated over a low-q range using the result of the cumulant expansion:

$$\ln(|S(q)|) = -\frac{1}{2}\sigma^2 q^2 + \frac{1}{24}\mu^4 q^4, \quad (10)$$

$$\theta(q) = \langle\zeta\rangle q - \frac{1}{6}\gamma^3 q^3, \quad (11)$$

where σ^2, γ^3, and μ^4 represent the second, third and fourth central moments, respectively, often referred to as variance, skewness, and kurtosis. The low-q signal may only be accurately represented by a truncated cumulant expansion if free of systematic residuals, as can arise from broken Hermitian symmetry due to experimental artefacts. If the non-Hermitian component is only a small fraction of the signal, the signal may be symmetrized using the method outlined by Scheven et al. [25]. Systematic residuals may also be introduced if the data cannot be accurately described by a truncated cumulant expansion. To eliminate the introduction of residuals, a maximum fit range is evaluated through analysis of the quality of the fit (Q) for an increasing range of q-space using methods described elsewhere [25]. A critical value of Q is defined, Q_c, below which the fit is considered unacceptable. The maximum fit range $|q_{\max}|$ is the maximum range for which $Q > Q_c$.

A non-linear least squares regression of Eqs. (10) and (11) is then performed across an increasing range of q-space to the limit of $|q_{\max}|$, with lower limits on the fit range defined as $2^{-1/2}$ $|q_{\max}|$ for the log-magnitude and $2^{-1/3}$ $|q_{\max}|$ for the phase of the q-space signal, as proposed in the literature [25], yielding multiple cumulants. The cumulants reported in this paper are the mean cumulant values and the errors are the standard deviation of the cumulants. If the limit of $|q_{\max}|$ is not reached, the value of $|q_{\max}|$ can be assumed to equal the maximum value of q-space sampled. Eqs. (7)–(9) were used to simulate q-space data for a suitable range of

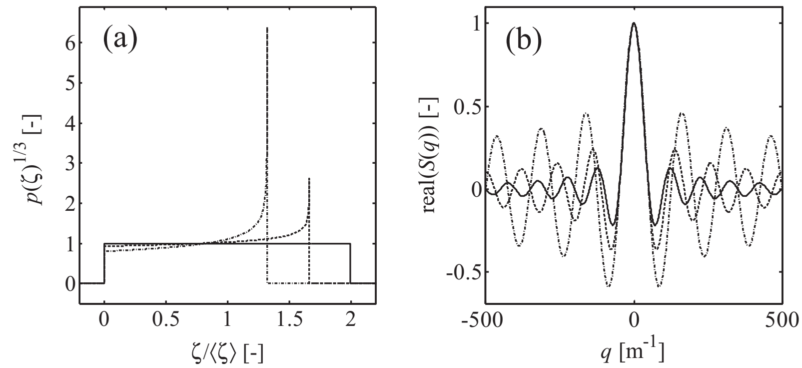

Fig. 2. (a) Displacement probability distributions (cube-root of probability is plotted for clarity) and (b) the evolution of the real component of the signal (scaled as a ratio of the maximum signal intensity) over a high-q range for three different flow behaviour indices; (—) $n = 1$, (- -) $n = 0.5$, and (-·-) $n = 0.2$. The NMR signal was simulated with parameters $\langle\zeta\rangle = 5$ mm, $\Delta = 100$ ms, and $D = 0$ m^2 s^{-1}.

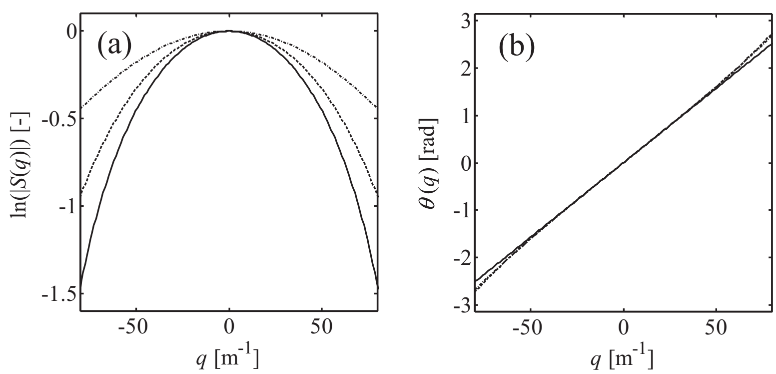

Fig. 3. The evolution of the (a) log-magnitude and (b) phase of the signal over low-q for three flow behaviour indices; (—) $n = 1$, (- -) $n = 0.5$, and (-·-) $n = 0.2$, where $\langle\zeta\rangle = 5$ mm, $\Delta = 100$ ms, and $D = 0$ m^2 s^{-1}.

flow behaviour indices, with typical experimental parameters. Using the methods outlined previously, cumulants for all flow behaviour indices were then obtained from the simulated q-space data. The relationship between cumulants and the flow behaviour index is shown in Fig. 4 for (a) variance, (b) skewness, and (c) kurtosis, with variance observed to be unique in its solution of n. If we assume a Gaussian distribution of cumulants corresponding to the increasing fit range, a flow behaviour index probability distribution can be produced for each cumulant using the mean cumulant value and the standard deviation of the cumulants.

The product of the three distributions, denoted $p(n)$ and given by $p(n, \sigma^2)p(n, \gamma^3)p(n, \mu^4)$, gives the overall distribution. The flow behaviour indices reported in this paper correspond to the weighted mean and unbiased estimates of the standard deviation of the flow behaviour index calculated from $p(n)$.

3. Materials and methods

3.1. Experimental

3.1.1. Materials

Aqueous solutions of xanthan gum (Sigma Aldrich, UK) were prepared in concentrations of 0.2, 0.4, and 0.6 wt% using deionised water (ELGA Purelab Option). These concentrations were selected to ensure power-law rheology across a suitable range of shear rates [28]. Complete dissolution of xanthan gum was achieved by stirring for 8 h using an overhead stirrer (Ika-Werke RW20); care was taken to prevent air entrapment during this process.

The flow system, consisting of a 14 mm internal diameter (i.d.) Perspex pipe of length 2 m and approximately 8 m of 10 mm i.d. PVC tubing with a total loop volume of 1.5 L, was operated in a closed loop configuration. A peristaltic pump (MasterFlex Console Drive) capable of delivering flow rates of up to 50 mL s^{-1} was used, and steady flow was ensured through coupling of the pump with a flow pulsation dampener. The radiofrequency (r.f.) coil was situated 1.5 m downstream of the pipe inlet, exceeding an inlet length of 60 times pipe i.d. recommended to ensure developed flow [29]. Experiments were performed at a flow rate of 11.5 ± 0.5 mL s^{-1} to produce a mean velocity of 75 ± 4 mm s^{-1}. This is within the laminar flow regime which is typically observed for Reynolds numbers up to 2000 [29].

3.1.2. Magnetic resonance

All experiments were performed on a Bruker AV85 spectrometer operating with a 2 T horizontal-bore superconducting magnet. The magnet was fitted with a 60 mm i.d. birdcage r.f. coil tuned to a frequency of 85.2 MHz for the ^{1}H resonance. A three-axis gradient system with a maximum gradient strength of 10.7 G cm^{-1} was used for spatial and flow encoding.

A 13-interval alternating pulsed field gradient stimulated echo (APGSTE) pulse sequence was used, as shown in Fig. 5, to acquire the high-q data required to obtain a full flow propagator, and the low-q data for cumulant analysis. The two sets of data are not acquired simultaneously due to the sampling requirements outlined in Section 1. To obtain the full flow propagator, gradient pulses with 2 ms duration (δ) and 40 ms separation (Δ) were applied and the flow-encoding gradient magnitude g was incremented linearly between ±6.0 G cm^{-1} in 128 steps (N), to sample a q-space range of ±5100 m^{-1}. This provided a FOF of 310 mm s^{-1} which exceeded the maximum expected velocity, thus satisfying

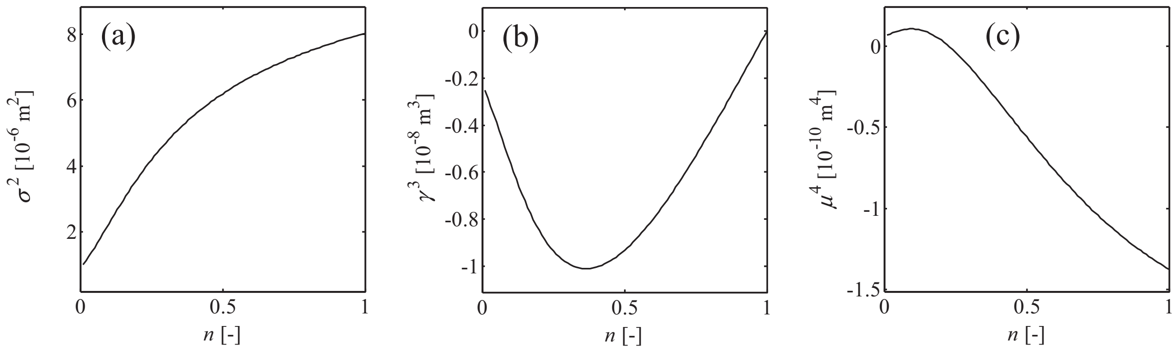

Fig. 4. (a) Variance, (b) skewness, and (c) kurtosis plotted as a function of the flow behaviour index, for simulated data where $\langle \zeta \rangle$ = 5 mm, Δ = 100 ms, and $D = 0\ \mathrm{m^2\,s^{-1}}$.

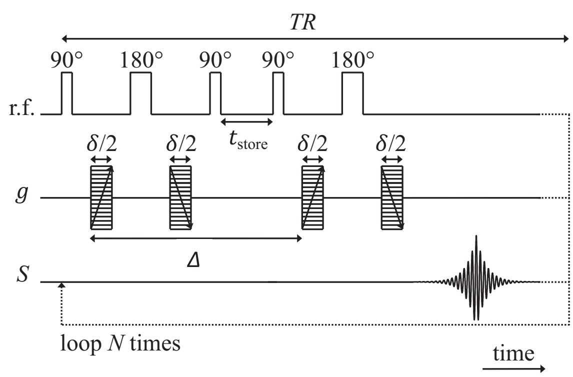

Fig. 5. A schematic for the 13-interval APGSTE sequence used for the acquisition of the volume-averaged flow propagator and low-q data.

one requirement of the Fourier transform. Parameters were held constant for all aqueous xanthan gum concentrations. A recycle time (TR) of 10 s, equal to ~4 times T_1, was utilised to give an acquisition time of 85 min with 4 signal averages. To obtain the low-q data in the range $\pm 106\ \mathrm{m^{-1}}$, gradient pulses were applied with δ = 0.5 ms and Δ = 50 ms. The gradient magnitude was incremented linearly in 128 steps between $\pm 0.5\ \mathrm{G\,cm^{-1}}$ to give an acquisition time of 85 min with TR = 10 s and 4 signal averages. These acquisition parameters were used for all samples. Much shorter acquisition times can be achieved when fewer gradient increments are required for the data analysis, as shown in Section 4, or by using fast velocity encoding techniques [14–16]. To validate the accuracy of the PFG-NMR measurements, spatially-resolved velocity images were acquired for each of the aqueous xanthan gum concentrations using a simple slice selective spin-echo flow MRI sequence [30], with a slice thickness of 10 mm. Data were acquired with SNR = 100. A field-of-view of 18 mm was selected in both the read and phase directions with 128 phase increments and 128 read points, to give a resolution of 141 μm × 141 μm. Flow-encoding gradients were applied with δ = 2 ms and Δ = 20 ms, and two increments in gradient magnitude were utilised with the magnitude calibrated for each sample to ensure a maximum phase shift of 2π. The acquisition time for the velocity image was 45 min with a TR of 2.6 s and four signal averages. For quantification of the velocity images, a zero velocity image was also acquired for each sample giving a total acquisition time of 90 min. All experiments were performed at 19.0 ± 0.5 °C.

3.1.3. Conventional rheometry

Measurements of the flow behaviour index were validated using a Rheometric Scientific ARES 320 rheometer. A smooth-walled concentric cylinder Couette cell, with inner cylinder of outer diameter 32 mm and length 34 mm, was used for all samples. The wall gap was 1 mm and the temperature was maintained at 19.0 ± 1.0 °C. The rheometer was operated in controlled-shear mode, with stress measured during a two-way shear rate sweep of between 500 and 0.01 $\mathrm{s^{-1}}$.

3.2. Simulations

Simulations were performed in MATLAB 2012b, operating under Windows 7. To examine the sensitivity of this technique to important experimental parameters, data were generated by the addition of pseudo-random Gaussian noise in quadrature, with zero mean and standard deviation σ, to noise-free data obtained using Eq. (9):

$$\frac{S(q,n)}{S(0)} = \int p'(\zeta,n) e^{iq\zeta - 4\pi^2 D\left(\Delta - \frac{\delta}{3}\right)q^2} \mathrm{d}\zeta + e(q), \tag{12}$$

where $e(q)$ represents the noise in the signal. SNR is here defined as the ratio of the signal intensity in the centre of q-space to the standard deviation of the noise. Simulation parameters, including gradient pulse timings and magnitudes, were identical to the experimental parameters outlined in Section 3.1.2 for the acquisition of low-q data. Remaining parameters are defined as follows:

- The value of ζ_{max} was determined by evaluating Eq. (3) at $r = 0$ for each value of flow behaviour index, and $p'(\zeta, n)$ was determined for 2^{15} linear increments of ζ between zero and ζ_{max}, with ζ = 3.57 mm, agreeing with that used experimentally.
- The flow behaviour index was increased linearly between 0.1 and 1 in 10 steps, corresponding to a shear rate range of 0–1000 $\mathrm{s^{-1}}$ for a pipe diameter of 14 mm.
- q-space was linearly sampled between the minimum and maximum values, defined by the gradient timings and magnitude, using 2^A points, with A taking integer values between 1 and 10 (to sample 2–2048 points).
- Noise was incremented linearly between 0% and 10% in 11 steps, corresponding to a SNR range of 10–∞.

Simulations using cumulant analysis were performed 10^2 times, each with pseudo-random Gaussian noise, for all combinations of experimental parameters. Mean cumulants and the weighted mean flow behaviour index were determined for each repetition using methods outlined in Section 2, and the simulation values reported are the mean and standard deviation of the mean cumulants and weighted mean flow behaviour indices, respectively. To generate the cumulant data for comparison with experimental data, 150 increments in the flow behaviour index were utilised evenly spaced between 0.01 and 1.50 to provide a resolution in the flow behaviour index of 0.01.

4. Results and discussion

4.1. Sensitivity to the flow behaviour index

The sensitivity of the cumulant analysis technique to the flow behaviour index is demonstrated in Fig. 6, which shows the mean variance and error associated with flow behaviour indices of 0.1–1 for (a) 256 and (b) 16 q-space data points, linearly sampled between ±106 m^{-1}, with SNR of (i) ∞, (ii) 100, and (iii) 50. As seen in Fig. 6, the mean variance values remain approximately constant, deviating from unity by less than ±1%, thus indicating an absence of systematic error and robustness to changes in experimental parameters, as well as n. In contrast, the error increases with a reduction in the flow behaviour index, reduction in the SNR, and reduction in the number of sampled q-space data points; for 16 sampled q-space data points and SNR of 50, the error in the measurement of variance is reduced from 7% to 4% as the flow behaviour index increases from 0.1 to 1. Similar trends are observed for skewness and kurtosis.

Using the methods proposed in Section 2, the mean and standard deviation of the weighted mean flow behaviour indices were determined from the cumulants. Fig. 7 compares the expected n to that predicted using cumulant analysis, for (a) 256 and (b) 16 q-space data points, linearly sampled between ±106 m^{-1}, and SNR of (i) ∞, (ii) 100, and (iii) 50, with the error bars equal to the standard deviation. The mean predicted flow behaviour index deviates from the expected index by less than ±2%, with the highest errors associated with SNR of 50 and 16 sampled data points, but the error changes considerably across the range of parameters investigated, increasing with a reduction in SNR and reduction in the number of sampled q-space data points. Fluctuations in the error are seen as n_i varies, however, these fluctuations are minimal when compared to those induced as a result of changes in SNR and the number of sampled q-space data points. The accuracy of the characterisation is, therefore, largely insensitive to the flow behaviour index.

4.2. Sensitivity to SNR and number of sampled q-space data points

Fig. 8 illustrates the error associated with the characterisation as a function of both noise and the number of sampled q-space data points, for (a) $n = 0.1$ and (b) $n = 1.0$. Noise is defined as the noise-to-signal ratio represented as a percentage, such that an SNR of 100 is equal to 1% noise, where the signal magnitude is taken at $q = 0\ m^{-1}$. As expected, it is seen that, for a given accuracy of characterisation, the sampling requirement is highly dependent upon the noise level. For the experiments reported here, utilising a 2 T magnet, an SNR of 10,000 was typical. Under these conditions, only 4 data points are required to be sampled in q-space to provide an error of less than 5%. This represents a 97% reduction in the acquisition time using the approach proposed in this paper to characterise n, when compared with the acquisition of a full flow propagator with 128 phase encoding steps. As the noise increases, an increasing number of data points are required to achieve the same error, and for a noise level of 2%, 128 points are required to provide an error less than 5%. The results are in good agreement with previous work [25] and further demonstrate the robustness of cumulant analysis to reductions in SNR, with the degree of robustness to SNR dependent upon the number of sampled q-space data points. For a noise level of <1%, if an error of less than 5% is required in the measurement and $n = 0.1$, only 8 points are required. These results are significant as they imply that the technique can be used to determine quantitative rheological parameters on low field hardware, and even potentially Earth's Field NMR systems. On such systems, the low SNR associated with spatially-resolved measurements may render spatially-resolved measurements of velocity inaccurate and/or impractical.

4.3. Magnetic resonance displacement probability distributions

Volume-averaged flow propagators were acquired for each aqueous xanthan gum concentration at a flow rate of $11.5 \pm 0.5\ mL\ s^{-1}$. Shown in Fig. 9 are the flow propagators obtained for gum concentrations of (a) 0.0, (b) 0.2 and (c) 0.6 wt%. A correction was applied to the experimentally acquired flow propagators, in the form of Eq. (8), to recover $p(\zeta)$. As seen in Fig. 9, an increase in the xanthan gum concentration from 0 to 0.6 wt% is responsible for a reduction in the maximum velocity from $\sim$150 to $\sim$100 $mm\ s^{-1}$, and an increase in the maximum probability, thus indicating a reduction in the flow behaviour index, i.e. an increase in shear-thinning behaviour. This trend is in agreement with the literature [31]. The flow rate calculated from the flow propagators was $12.8 \pm 0.5\ mL\ s^{-1}$, with the error a result of the propagators demonstrating Gibbs ringing due to a truncation of the acquired signal in q-space. These artefacts are more pronounced with a reduction in the flow behaviour index due to the emergence of a dominant spike in the flow propagator. As the propagator approaches a shifted delta function, the signal acquired in q-space tends to a cosine function, as is observed in Fig. 2(b), and so truncation of the signal is inevitable at lower values of flow behaviour index. Truncation artefacts could be minimised through apodisation of the acquired signal before Fourier transform, however, this would cause a loss in propagator resolution.

4.4. Magnetic resonance and cumulant analysis

The signal in q-space was acquired over a low-q range for the purpose of cumulant analysis. Symmetrisation of the complex acquisition data was performed using methods outlined in the literature [25]. The non-linear least squares regression of Eqs. (10) and (11) to the symmetrised log-magnitude and phase q-space data, respectively, yielded cumulants that varied with the flow behaviour index, as was demonstrated in Fig. 4. Analysis of the fit quality across an increasing range of q-space showed that $|q_{max}|$, the maximum fitting range, was not exceeded for any sample investigated, and so the regression was performed across the full range of ±106 m^{-1}. Cumulants were generated for flow behaviour indices of 0.01–1.50 using the simulation method outlined previously in Section 2, and compared with those determined experimentally. Using this approach, the flow behaviour indices were characterised for the range of aqueous xanthan gum concentrations investigated experimentally, all of which indicated shear-thinning behaviour. Across the shear rate range of the NMR experiments (0–100 s^{-1}), the flow behaviour indices were 1.01 ± 0.03, 0.39 ± 0.01, 0.23 ± 0.01, and 0.15 ± 0.01 for aqueous xanthan gum concentrations of 0, 0.2, 0.4, and 0.6 wt%, respectively, where the error represents the unbiased standard deviation of the flow behaviour index probability distribution.

An increase in xanthan gum concentration is responsible for a reduction in the flow behaviour index, as observed using the flow propagators, and the flow behaviour index of the 0 wt% sample is in agreement with that expected for a Newtonian fluid. A comparison of the experimental and regression data is shown in Fig. 10 for an aqueous xanthan gum concentration of 0.2 wt%, with the fit accurate to within the accuracy of the experimental data. Furthermore, if we now examine the influence of the number of sampled q-space data points on the weighted mean flow behaviour index obtained, as shown in Fig. 11 for an aqueous xanthan gum concentration of 0.2 wt%, we observe that even with only 8 sampled q-space data points the error associated with n is less than 3%. The limiting value of flow behaviour index, n_l, is reached at

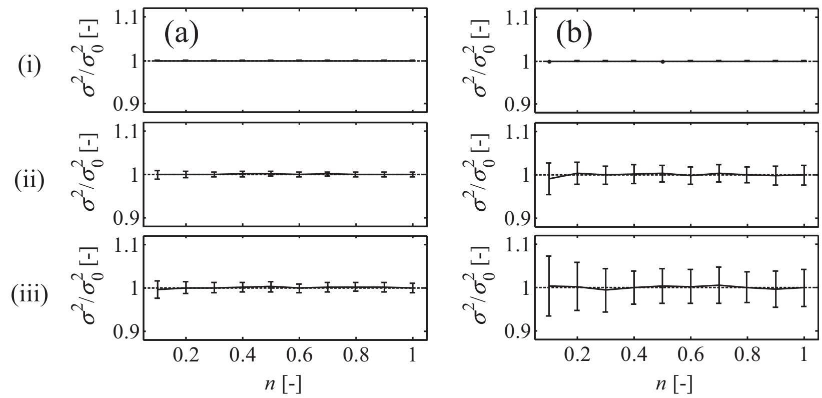

Fig. 6. Plots to demonstrate the relationship between mean variance (represented as a fraction of the zero-noise mean variance, σ_0^2) and the flow behaviour index. Data are plotted for (a) 256 and (b) 16 sampled q-space data points, with SNR of (i) ∞, (ii) 100, and (iii) 50. Error bars represent the standard deviation of the variances generated from 100 simulations.

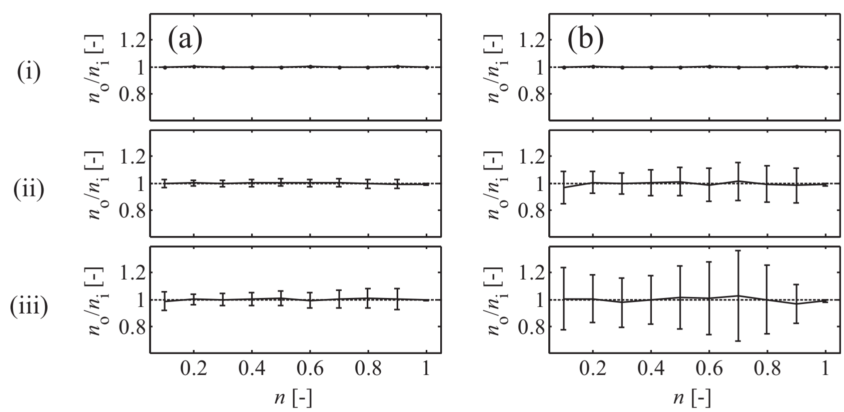

Fig. 7. Plots to compare the expected (input, n_i) flow behaviour index and that recovered (output, n_o) using cumulant analysis for a range of index values, for (a) 256 and (b) 16 sampled q-space data points and SNR of (i) ∞, (ii) 100, and (iii) 50. The error bars represent uncertainties in the flow behaviour index due to uncertainties in the measured variance.

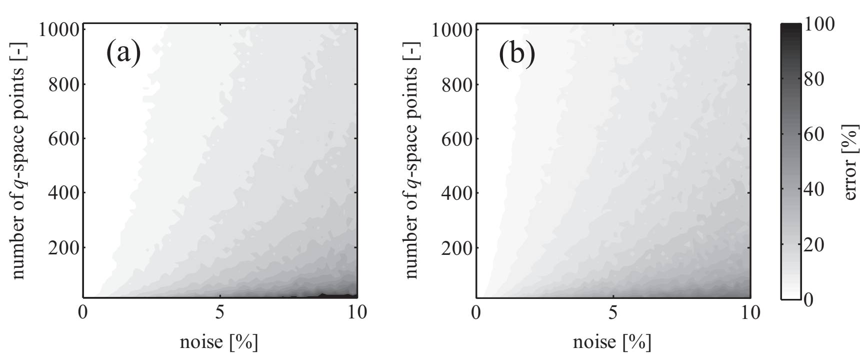

Fig. 8. Two-dimensional contour plots demonstrating the uncertainty (error) associated with the flow behaviour index for the range of SNR and number of sampled q-space data points investigated, for flow behaviour indices of (a) 0.1 and (b) 1, using 64 increments in both noise and number of sampled q-space data points.

~40 data points and, therefore, the acquisition of 128 points increases the acquisition time but does not enhance the accuracy of the characterisation. This result demonstrates that a reduction in acquisition time from 85 min to 5 min is possible when using the cumulant analysis approach compared to the acquisition of a volume-averaged flow propagator with 128 phase encoding steps. There are potential time savings associated with the proposed cumulant analysis approach when compared to flow MRI, however, a quantitative assessment of the time savings is difficult and will not be considered here.

4.5. Flow MRI

Full two-dimensional (2D) velocity images were acquired for each aqueous xanthan gum concentration with a spatial resolution of 141 μm × 141 μm, sufficient to provide ~100 spatially-resolved velocity data points across the geometry under study. Fig. 12 shows velocity image data for aqueous xanthan gum concentrations of (a) 0, (b) 0.2, and (c) 0.4 wt%, where the velocity represents axial velocity, i.e. z-velocity. The SNR in the images is 100. Flow rates calculated from the velocity images (11.6 ± 0.4 mL s^{-1})

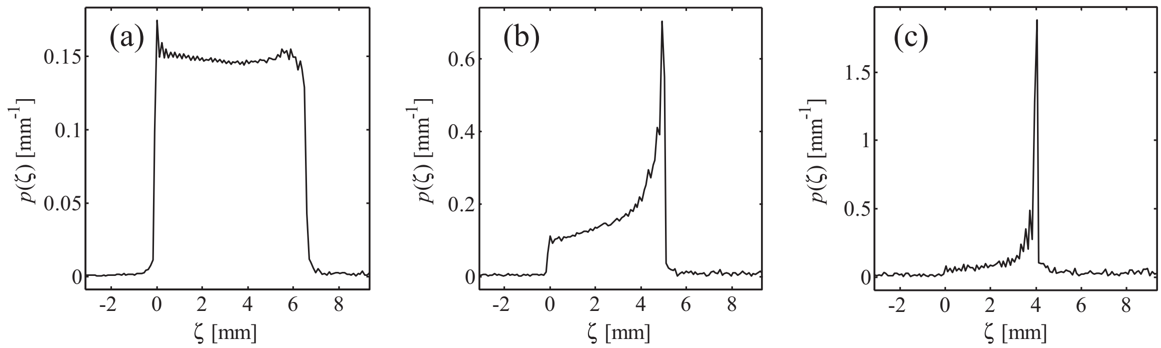

Fig. 9. Plots to show volume-averaged experimentally-acquired flow propagators for (a) 0.0, (b) 0.2 and (c) 0.6 wt% aqueous xanthan gum, acquired in 85 min. The propagators demonstrate a reduction in maximum velocity and increase in maximum probability for an increase in gum concentration. An increase in truncation artefacts is observed as the xanthan gum concentration is increased from 0.0 to 0.6 wt% due to the propagator approaching a shifted delta function, this corresponding to a cosine signal in q-space.

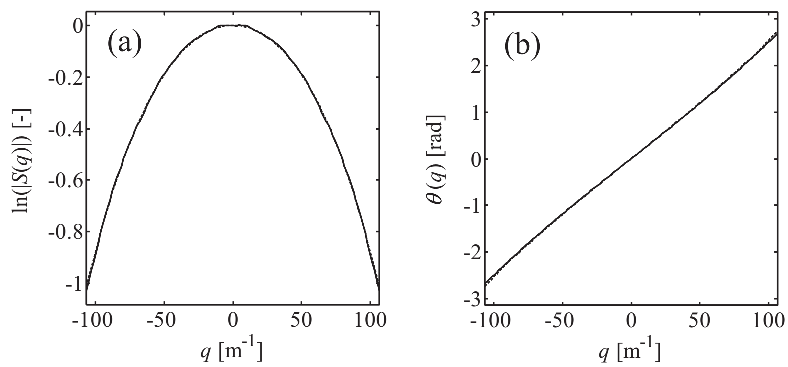

Fig. 10. Plots to show the (a) log-magnitude and (b) phase of the q-space data for 0.2 wt% aqueous xanthan gum. Included on the plots are both the (—) experimental and (- -) regression data with $n = 0.39$; the two datasets overlap.

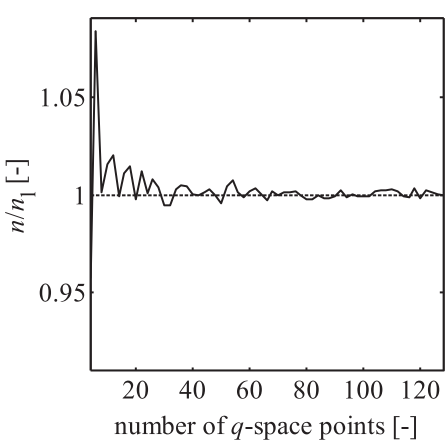

Fig. 11. The flow behaviour index, n, plotted as a ratio of the flow behaviour index at 128 points, termed the limiting flow behaviour index and denoted n_l, for 0.2 wt% aqueous xanthan gum. The increasing number of q-space data points is sampled linearly between $\pm 106\ \mathrm{m}^{-1}$. The flow behaviour indices were calculated using cumulants determined from a single least-squares regression to the experimental data.

suggest this technique to be accurate to within the limits of the error of the macroscopic flow measurement ($11.5 \pm 0.5\ \mathrm{mL\ s^{-1}}$). The maximum velocity for 0 wt% aqueous xanthan gum solution was observed to have a value of $154\ \mathrm{mm\ s^{-1}}$, also within the experimental error assuming a parabolic velocity profile ($150 \pm 8\ \mathrm{mm\ s^{-1}}$), corresponding to a Reynolds number of $\sim$1100. A transition to the turbulent flow regime is typically observed between Reynolds numbers of 2000–4000 [29]. As expected, the velocity images do not demonstrate any of the features attributed to turbulent flow, with the velocity images showing the radial symmetry typical of laminar flow.

The flow behaviour index was characterised by performing a non-linear 2D regression of $\Delta^{-1}\zeta(r)$ to the velocity image data, with $\zeta(r)$ given by Eq. (3). This non-linear regression is depicted in 1D in Fig. 13 by means of velocity profiles generated using radially averaged 2D velocity image and regression data. The experimental data and fitted data shown in Fig. 13 are in excellent agreement to within the accuracy of the experimental data for all aqueous xanthan gum concentrations investigated, confirming power-law rheology over the shear rate range of the NMR experiments (1–100 $\mathrm{s^{-1}}$). Using this method, the flow behaviour index was found to be 0.99 ± 0.04, 0.39 ± 0.02, 0.25 ± 0.01, and 0.15 ± 0.01 for aqueous xanthan gum concentrations of 0, 0.2, 0.4, and 0.6 wt%, respectively, where the error is representative of a 95% confidence interval in the individual fit. The flow behaviour indices determined using cumulant analysis are in agreement to within 8% of those found using flow MRI, and absent of any systematic error. The cumulant analysis technique proposed in this paper therefore offers a new approach to rheological characterisation using NMR, with a potential increase in temporal resolution enabling rapid perturbations in flow behaviour index to be identified. Furthermore, the requirement of more expensive gradient hardware is negated, with this technique requiring only a single axis low-power gradient system. This approach could be applied on low field, portable hardware due to the robustness demonstrated by cumulant analysis to poor SNR.

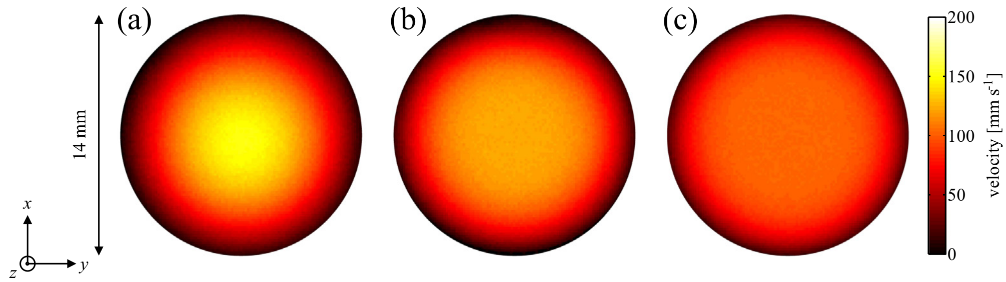

Fig. 12. Two-dimensional z-velocity images acquired for (a) 0, (b) 0.2, and (c) 0.4 wt% aqueous xanthan gum with a flow rate of 11.5 ± 0.5 mL s^{-1}. The images have a spatial resolution of 141 μm × 141 μm and were acquired in 90 min. The SNR in the intensity images is 100.

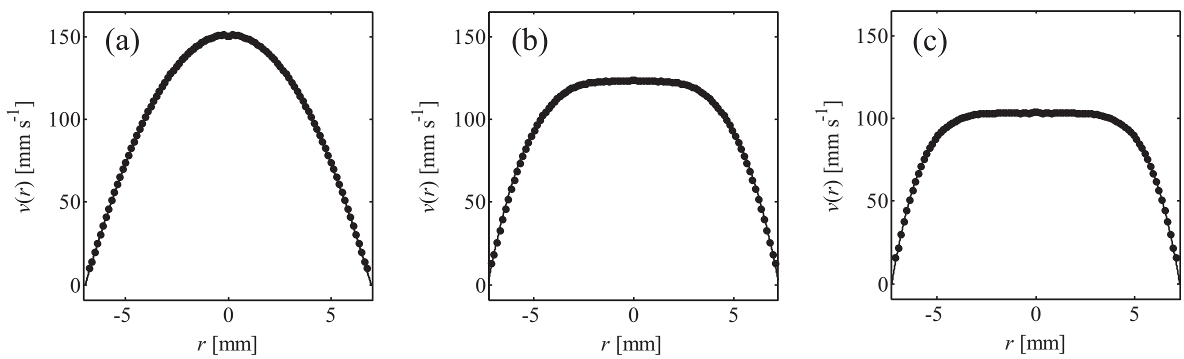

Fig. 13. Velocity profiles for (a) 0, (b) 0.2, and (c) 0.4 wt% aqueous xanthan gum showing the radially averaged velocity image data (●). The solid lines (–) correspond to the radially averaged regression data obtained by performing a non-linear 2D regression of $\Delta^{-1}\zeta(r)$ to the velocity image data, with $\zeta(r)$ given by Eq. (3). The error in the fitted data is within the accuracy of the experimental data.

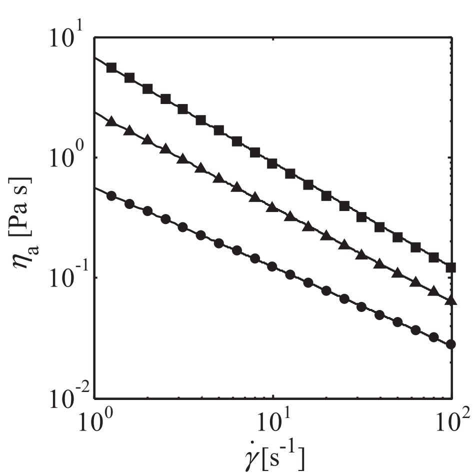

Fig. 14. Apparent shear viscosity η_a against shear rate $\dot{\gamma}$ for (●) 0.2, (▲) 0.4, and (■) 0.6 wt% aqueous xanthan gum plotted across the shear rate range of the NMR experiments. The data were acquired using conventional rheometry methods with a shear rate sweep of 0.01–500 s^{-1}. Solid lines represent the non-linear regression of the data with Eq. (13), fitted across the range 1–100 s^{-1}, with consistency indices of 0.560 ± 0.002, 2.36 ± 0.01, 6.73 ± 0.03 Pa s^n for 0.2, 0.4, and 0.6 wt% aqueous xanthan gum, respectively, and flow behaviour indices as described in Section 4.6.

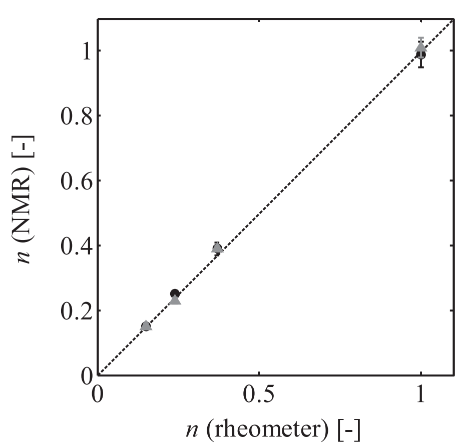

Fig. 15. A comparison of the flow behaviour indices calculated using the three methods, with those determined using (●) flow MRI and (▲) cumulant analysis plotted against those determined using conventional rheometry. For comparison, all flow behaviour indices were calculated across a shear rate range of 1–100 s^{-1}. The dashed line (- -) describes the ideal trendline, i.e. $y = x$, and the error bars represent the uncertainty in the measurement of the flow behaviour index.

4.6. Conventional rheometry

To validate the results of NMR methods, rheological characterisation was also performed on conventional rheometry apparatus. Stress was measured across a shear rate sweep of 0.01–500 s^{-1} and the measured apparent shear viscosity-shear rate curves for 0.2, 0.4, and 0.6 wt% aqueous xanthan gum solutions studied are shown in Fig. 14 across the shear rate range of the NMR experiments. Shear viscosity is defined as the shear stress to shear rate ratio. At low values of shear rate a flattening of the curves was observed, with the shear viscosity approaching the low-shear viscosity. As expected, an increase in the xanthan gum concentration caused an increase in the low-shear viscosity. For all samples investigated, an increase in the shear rate causes a reduction in the shear viscosity, indicating shear-thinning behaviour. This is in great agreement with trends observed using NMR techniques.

The apparent shear stress measured by the rheometer is given, for a fluid demonstrating power-law rheology, by:

$$\tau_a = \left(\frac{4}{3+n}\right)k\dot{\gamma}^n, \tag{13}$$

where τ_a is the apparent shear stress. All fluids investigated demonstrated excellent agreement to the power-law model across a shear rate range of 1–200 s^{-1}, the same order magnitude as those of the NMR experiments (1–100 s^{-1}). The non-linear regression of Eq. (13) to the apparent shear stress–shear rate data across the shear rate range of the NMR experiments yielded flow behaviour indices of 1.00 ± 0.01, 0.37 ± 0.01, 0.24 ± 0.01, and 0.15 ± 0.01 for 0, 0.2, 0.4, and 0.6 wt%, respectively, where the error is representative of a 95% confidence interval in the individual fit. The flow behaviour indices determined using this method are compared with those using spatially-resolved NMR and cumulant analysis in Fig. 15, with the results from the three methods observed to be in agreement to within 5%.

5. Conclusions

In this paper, a new PFG-NMR analysis approach was proposed enabling the characterisation of the flow behaviour index using a cumulant analysis. An expression describing the signal acquired in q-space in terms of the flow behaviour index, n, was used to systematically investigate parameters of interest including SNR, number of sampled q-space data points, and the flow behaviour index. It was shown that cumulant analysis is robust to reductions in the number of sampled q-space data points and reductions in SNR. An increase in temporal resolution of the proposed approach is possible through a reduction in the number of sampled points when compared to the acquisition of a full flow propagator, with the reduction limited by the SNR of the system.

To validate this proposed PFG-NMR and cumulant analysis approach we have shown excellent agreement (to within 8%) between the flow behaviour indices obtained using the cumulant analysis and flow MRI data; these indices were then demonstrated to be in agreement, within 5%, of the same quantities determined by conventional rheometry. All flow behaviour indices quoted were characterised across a shear rate range of 1–100 s^{-1}.

Using this approach we have shown that with SNR as low as 50, quantitative results can be acquired to within 5% when 128 q-space points are sampled. This can be reduced to as low as 8 q-space points for SNR of 100 to obtain results of the same accuracy, and only 4 points with SNR >10,000.

An obvious implication of this is that the requirement of only a single-axis, low-power gradient system removes the need for more expensive hardware for the MR characterisation of non-Newtonian fluids. Furthermore, the robustness of this approach to SNR <100 opens up opportunities for use with low field, portable hardware.

Acknowledgments

AJS wishes to thank the EPSRC (grant numbers EP/F047991/1 and EP/K039318/1) and TB wishes to thank the EPSRC and Johnson Matthey plc for financial support. We also thank Dr. Simon Butler for the provision of and assistance with conventional rheological measurements. Additional data related to this publication is available at https://www.repository.cam.ac.uk/handle/1810/247295.

References

[1] P.T. Callaghan, Rheo-NMR and velocity imaging, Curr. Opin. Colloid Interface Sci. 11 (2006) 13–18.
[2] D.F. Arola, R.L. Powell, G.A. Barrall, M.J. McCarthy, A simplified method for accuracy estimation of nuclear magnetic resonant imaging, Rev. Sci. Instrum. 69 (1998) 3300–3307.
[3] D.F. Arola, G.A. Barrall, R.L. Powell, K.L. McCarthy, M.J. McCarthy, Use of nuclear magnetic resonance imaging as a viscometer for process monitoring, Chem. Eng. Sci. 52 (1997) 2049–2057.
[4] A.J. Sederman, M.D. Mantle, C. Buckley, L.F. Gladden, MRI technique for measurement of velocity vectors, acceleration, and autocorrelation functions in turbulent flow, J. Magn. Reson. 166 (2004) 182–189.
[5] P. Galvosas, P.T. Callaghan, Fast magnetic resonance imaging and velocimetry for liquids under high flow rates, J. Magn. Reson. 181 (2006) 119–125.
[6] A.B. Tayler, D.J. Holland, A.J. Sederman, L.F. Gladden, Time resolved velocity measurements of unsteady systems using spiral imaging, J. Magn. Reson. 211 (2011) 1–10.
[7] T.M. Osán, J.M. Ollé, M. Carpinella, L.M.C. Cerioni, D.J. Pusiol, M. Appel, J. Freeman, I. Espejo, Fast measurements of average flow velocity by low-field ^{1}H NMR, J. Magn. Reson. 209 (2011) 116–122.
[8] H. Herold, E.H. Hardy, M. Ranft, K.-H. Wassmer, N. Nestle, Online Rheo-TD NMR for analysing batch polymerisation processes, Micropor. Mesopor. Mater. 178 (2013) 74–78.
[9] H.Y. Carr, E.M. Purcell, Effects of diffusion on free precession in NMR experiments, Phys. Rev. 94 (1954) 630–638.
[10] E.L. Hahn, Spin echoes, Phys. Rev. 80 (1954) 580–594.
[11] P.T. Callaghan, Principles of Nuclear Magnetic Resonance Microscopy, Clarendon Press, Oxford, 1993.
[12] K.J. Packer, The study of slow coherent molecular motion by pulsed nuclear magnetic resonance, Mol. Phys. 17 (1969) 355–368.
[13] J.E. Maneval, R.L. Powell, M.J. McCarthy, K.L. McCarthy, Magnetic resonance imaging of multiphase systems, particulate and two phase flow, Butterworth-Heinemann, Boston, 1993.
[14] T. Grover, J.R. Singer, NMR spin-echo flow measurements, J. Appl. Phys. 42 (1971) 938–940.
[15] A.N. Garroway, Velocity measurements in flowing fluids by MNR, J. Phys. D Appl. Phys. 7 (1974) L159–L163.
[16] J.P. Stamps, B. Ottink, J.M. Visser, J.P.M. van Duynhoven, R. Hulst, Difftrain: a novel approach to a true spectroscopic single-scan diffusion measurement, J. Magn. Reson. 151 (2001) 28–31.
[17] M.J. McCarthy, J.E. Maneval, R.L. Powell, Structure/property measurements using magnetic resonance spectroscopy and imaging, Advances in Food Engineering, CRC Press, Florida, 1992.
[18] J.D. Seymour, J.E. Maneval, K.L. McCarthy, R.L. Powell, M.J. McCarthy, Rheological characterization of fluids using velocity spectrum measurements, J. Texture. Stud. 26 (1995) 89–101.
[19] T. Chevalier, S. Rodts, C. Chevalier, P. Coussot, Quantitative exploitation of PFG NMR and MRI velocimetry data for the rheological study of yield stress fluid flows at macro- and micro-scales in complex geometries, Exp. Fluids 56 (2015) 1868.
[20] E.O. Stejskal, J.E. Tanner, Spin diffusion measurements: spin echoes in the presence of a time-dependent field gradient, J. Chem. Phys. 42 (1965) 288–292.
[21] J.E. Tanner, Use of stimulated echo in NMR-diffusion studies, J. Chem. Phys. 52 (1970) 2523–2526.
[22] J. Kärger, W. Heink, The propagator representation of molecular transport in microporous crystallites, J. Magn. Reson. 51 (1983) 1–7.
[23] A.A. Collyer, D.W. Clegg, Rheological Measurement, Springer, Netherlands, 1998.
[24] U.M. Scheven, D. Verganelakis, R. Harris, M.L. Johns, L.F. Gladden, Quantitative nuclear magnetic resonance measurements of preasymptotic dispersion in flow through porous media, Phys. Fluids 17 (2005) 117107.
[25] U.M. Scheven, J.P. Crawshaw, V.J. Anderson, R. Harris, M.L. Johns, L.F. Gladden, A cumulant analysis for non-Gaussian displacement distributions in Newtonian and non-Newtonian flows through porous media, Magn. Reson. Imaging 25 (2007) 513–516.
[26] H.A. Barnes, J.F. Hutton, An Introduction to Rheology, Elsevier, Amsterdam, 1989.
[27] L.G. Kaiser, J.W. Logan, T. Meersmann, A. Pines, Dynamic NMR microscopy of gas phase Poiseuille flow, J. Magn. Reson. 149 (2001) 144–148.
[28] K.G. Hollingsworth, M.L. Johns, Rheo-nuclear magnetic resonance of emulsion systems, J. Rheol. 48 (2004) 787–803.
[29] J.M. Coulson, J.F. Richardson, J.R. Backhurst, J.R. Harker, Coulson & Richardson's chemical engineering, Fluid Flow, Heat Transfer, and Mass Transfer, vol. 1, Butterworth-Heinemann, Oxford, 1999.
[30] L.F. Gladden, A.J. Sederman, Recent advances in Flow MRI, J. Magn. Reson. 229 (2013) 2–11.
[31] H.C.H. Bandulasena, B.Z. William, M.R. Julia, An inverse method for rheometry of power-law fluids, Meas. Sci. Technol. 22 (2011) 125402.